Endmember Extraction From Hyperspectral Imagery Based on Probabilistic Tensor Moments

Ruben Fernandez-Beltran, Filiberto Pla, and Antonio Plaza, *Fellow, IEEE*

***Abstract*— This letter presents a novel hyperspectral endmember extraction approach that integrates a tensor-based decomposition scheme with a probabilistic framework in order to take advantage of both technologies when uncovering the signatures of pure spectral constituents in the scene. On the one hand, statistical unmixing models are generally able to provide accurate endmember estimates by means of rather complex optimization algorithms. On the other hand, tensor decomposition techniques are very effective factorization tools which are often constrained by the lack of physical interpretation within the remote sensing field. In this context, this letter develops a new hybrid endmember extraction approach based on the decomposition of the probabilistic tensor moments of the hyperspectral data. Initially, the input image reflectance values are modeled as a collection of multinomial distributions provided by a family of Dirichlet generalized functions. Then, the unmixing process is effectively conducted by the tensor decomposition of the third-order probabilistic tensor moments of the multivariate data. Our experiments, conducted over four hyperspectral data sets, reveal that the proposed approach is able to provide efficient and competitive results when compared to different state-of-the-art endmember extraction methods.**

***Index Terms*— Endmember extraction, hyperspectral unmixing, statistical models, tensor decomposition.**

I. Introduction

HYPERSPECTRAL imaging (HSI) is one of the most important technologies to address many different applications within the remote sensing field [1]. In general, HSI sensors capture the Earth surface using hundreds of narrow and contiguous bands, providing valuable spectral and spatial information of the target scene [2]. Nonetheless, the higher the spectral precision of the sensor, the smaller the spatial resolution of the recorded data, since the amount of photons captured at each band logically decreases [3]. In this context, hyperspectral unmixing (HU) plays a fundamental role to uncover subpixel information from the sensed spectra because HU aims at decomposing HSI imagery into a collection of pure spectral signatures (endmembers) and a set of fractional abundances that represent pixel endmember proportions. From geometrical techniques to statistical models, different paradigms have been successfully applied to unmix remotely sensed data [4]. Geometrical approaches exploit the HSI data geometry to estimate the spectral signatures and fractional abundances. The vertex component analysis (VCA) [5] is one of the most popular and effective geometrical methods. Specifically, VCA assumes that the endmembers of a given HSI scene define a simplex of minimum volume that encloses the data. In this way, spectral signatures can be efficiently estimated using convex set geometry. Another relevant approach is the minimum volume simplex analysis (MVSA) [6], which introduces some additional constraints on the abundance fractions to increase the model robustness to the absence of pure pixels and also to the presence of noise. Statistical methods follow a probabilistic scheme to model endmembers and abundances as probability distributions, thus accounting for a higher data variability. For instance, in [7] Nascimento and Bioucas formulate fractional abundances as mixtures of Dirichlet densities. Similarly, other authors model the endmember variability using different distributions, such as the Gaussian distribution [8] or topic modeling [9]. Despite the remarkable performance achieved by these methods, alternative research work has also been conducted considering the data decomposition nature of the HU problem. In this sense, several papers in the literature adopt the nonnegative matrix factorization (NMF) approach [10], which aims at decomposing the input HSI data into two multiplicative factors, i.e., endmembers and abundances. For instance, this is the case of the work presented in [11], where the authors introduce different regularization constrains over the elemental NMF scheme. Analogously, Li *et al.* [12] propose a robust collaborative NMF (CNMF) approach, which is capable of working with an overestimated number of endmembers. As an alternative to the NMF scheme, some recent works show the advantages of considering a tensor-based decomposition framework, which allows preserving more spatial information, since the HSI data can be managed from a 3-D perspective. In this regard, Qian *et al.* [13] present a matrix-vector NMF (MVNTF) approach which is, to the best of our knowledge, the first method that employs a tensor-based scheme for HU. Other authors, such as Feng and Wang [14], propose some additional constraints over the seminal approach that provides certain performance advantages.With the recent emergence of multilinear algebra to represent remotely sensed HSI data, HU methods no longer depend on traditional matrix decomposition techniques to uncover spectral signatures and fractional abundances. However, the lack of physical interpretation of the factorization process itself is often a conceptual limitation that still forces current decomposition-based HU approaches to impose additional restrictions, e.g., the sum-to-one and

Manuscript received May 10, 2019; revised August 2, 2019 and November 11, 2019; accepted December 26, 2019. Date of publication January 13, 2020; date of current version November 24, 2020. This work was supported in part by the Generalitat Valenciana under Grant APOSTD/2017/007, in part by the Spanish Ministry of Economy under Grant ESP2016-79503-C2-2-P, Grant RTI2018-098651-B-C54, and Grant TIN2015-63646-C5-5-R, in part by the Junta de Extremadura under Grant GR18060, and in part by the European Union under the H2020 EOXPOSURE under Project 734541. *(Corresponding author: Ruben Fernandez-Beltran.)*

Ruben Fernandez-Beltran and Filiberto Pla are with the Institute of New Imaging Technologies, Universitat Jaume I, 12071 Castellón de la Plana, Spain (e-mail: rufernan@uji.es; pla@uji.es).

Antonio Plaza is with the Hyperspectral Computing Laboratory, Department of Technology of Computers and Communications, Escuela Politécnica, University of Extremadura, PC-10003 Cáceres, Spain (e-mail: aplaza@unex.es).

Color versions of one or more of the figures in this letter are available online at https://ieeexplore.ieee.org.

Digital Object Identifier 10.1109/LGRS.2019.2963114

nonnegativity abundance constraints [12]–[14]. In this sense, some recent statistical methods, such as [15]–[17], show the advantages of considering a probabilistic framework to deal with remotely sensed HSI imagery. In particular, assuming that the input data are sampled from a probability distribution makes the sum-to-one and nonnegativity conditions inherent to the solution because the output result naturally belongs to the corresponding probability simplex [9], [18]. In this scenario, this letter proposes a new endmember extraction approach which aims at combining a tensor-based decomposition scheme with a probabilistic framework in order to take advantage of both technologies when unmixing remotely sensed HSI data. On the one hand, the latest research based on tensors [13], [14] reveals that this kind of factorization is able to provide very competitive and efficient results within the HU field. Nonetheless, the tensor decomposition approach does not show a literal meaning when estimating spectral signatures, which may eventually limit its physical interpretation while forcing some additional constraints. On the other hand, the probabilistic interpretation of the unmixing process [9] makes the probabilistic scheme very useful to represent the HSI data, since the image pixels are probabilistically distributed over the endmember space. In order to achieve this goal, we initially formulate the HU problem considering that the HSI data can be effectively modeled according to the multinomial distributions provided by a family of Dirichlet generalized functions. Then, the unmixing process is conducted using the third-order probabilistic tensor moments of the multivariate data. Our experiments, conducted over four HSI data sets, show the proposed approach exhibits competitive performance when compared to different state-of-the-art methods available in the literature.

II. Methodology

A. Endmember Extraction Formulation

Let $\mathbf{X} \in \mathbb{R}^{B\times N}$ be a HSI image with N pixels and B bands. Let K be the number of endmembers of $\mathbf{X}$. The endmember extraction task consists of estimating the inherent set of spectral signatures from $\mathbf{X}$ as $\mathbf{S} = \{\mathbf{s}_1, \dots, \mathbf{s}_K\} \in \mathbb{R}^{B\times K}$. Considering the linear mixing model [4], it is possible to characterize each pixel $\mathbf{X}^{(i)}$ as a mixture of K endmembers

$$\mathbf{X}^{(i)} = \sum_{k=1}^{K} \mathbf{s}_k \mathbf{a}_k^{(i)} \tag{1}$$

where $\mathbf{a}_k^{(i)} \in \mathbb{R}$ denotes the fractional abundance of $\mathbf{s}_k$ in $\mathbf{X}^{(i)}$. In order to guarantee that fractional abundances lie on the corresponding K-dimensional probability simplex Δ^{K-1}, let us assume that the abundance vectors $\mathbf{a} = \{\mathbf{a}^{(1)}, \dots, \mathbf{a}^{(N)}\} \in \mathbb{R}^{K\times N}$ are independently drawn from a Dirichlet distribution with a concentration parameter $\alpha = \{\alpha_1, \dots, \alpha_K\}$, being $\alpha_0 = \sum_{k=1}^{K} \alpha_k$. Consequently, the contribution of the endmembers to the image bands at the ith pixel can be modeled using a multinomial distribution with parameters $\mathbf{a}^{(i)}$, and the corresponding pixel reflectance values can then be derived from the endmember vectors $\mathbf{s}_k \in \Delta^{B-1}$. The way we encode the HSI data is by expressing each $1/2^{16}$ reflectance fraction of each band as a binary vector [19]. Let $\{\mathbf{v}_1, \mathbf{v}_2, \dots, \mathbf{v}_B\} \in \mathbb{R}^{K\times B}$ be the standard coordinate basis for $\mathbb{R}^B$. Then, we characterize the F reflectance fractions of $\mathbf{X}$ as a set of column vectors $\{\mathbf{x}_1, \mathbf{x}_2, \dots, \mathbf{x}_F\} \in \mathbb{R}^{B\times F}$, which indicate the activation of the HSI bands. In other words, each reflectance fraction $\mathbf{x}_f$ of $\mathbf{X}$ is expressed by the standard coordinate basis vector $\mathbf{v}_j$ corresponding to the band where the fraction $\mathbf{x}_f$ was acquired. Note that this notation allows expressing the joint probabilities of the HSI reflectance fractions using the cross-moments of these vectors.

B. Probabilistic Tensor Cross-Moments

With the aforementioned problem formulation in mind, let us now define some properties of the hidden moments of the HSI data, following the general tensor decomposition theory for learning latent variable models [20]. Considering that the endmember mixture $\mathbf{a}$ is drawn from a Dirichlet distribution, the expected value of the kth element of this vector can be defined as follows:

$$\mathbf{E}[\mathbf{a}_k] = \frac{\alpha_k}{\alpha_0}. \tag{2}$$

According to the aforementioned notation, the expected value of a reflectance fraction $\mathbf{x}_1 \in \mathbb{R}^B$ conditioned to the endmember mixture vector $\mathbf{a}$ can be represented as

$$\mathbf{E}[\mathbf{x}_1|\mathbf{a}] = \sum_{k=1}^{K} \mathbf{s}_k \mathbf{a}_k. \tag{3}$$

Equation (3) shows the relationship between the observed data $\mathbf{x}_1$ and the spectral signatures $\mathbf{s}_k$. However, it requires knowledge on the abundance vectors $\mathbf{a}$, which are logically unknown. As a result, it can be considered the marginal expectation $\mathbf{E}[\mathbf{x}_1]$ to derive the following expression:

$$\mathbf{E}[\mathbf{x}_1] = \mathbf{E}[\mathbf{E}[\mathbf{x}_1|\mathbf{a}]] = \sum_{k=1}^{K} \frac{\alpha_k}{\alpha_0} \mathbf{s}_k. \tag{4}$$

This equation reveals that the moments of the observable data are useful to recover the endmember vectors $\mathbf{s}_k$. Nonetheless, the moments of a single reflectance fraction $\mathbf{x}_1$ do not provide information to estimate spectral signatures that cover the complete HSI domain. For this reason, we consider the cross-moments of pairs of reflectance fractions as follows:

$$\mathbf{E}[\mathbf{x}_1 \otimes \mathbf{x}_2] = \mathbf{E}[\mathbf{S}\mathbf{a} \otimes \mathbf{S}\mathbf{a}] \tag{5}$$

where the symbol $\otimes$ denotes the Kronecker product. Analogously, the third-order cross-moment of the data can be formulated as

$$\mathbf{E}[\mathbf{x}_1 \otimes \mathbf{x}_2 \otimes \mathbf{x}_3] = \mathbf{E}[\mathbf{S}\mathbf{a} \otimes \mathbf{S}\mathbf{a} \otimes \mathbf{S}\mathbf{a}]. \tag{6}$$

Once the cross-moments of the input reflectance data are represented in terms of $\mathbf{S}$ and $\mathbf{a}$, it is also possible to derive a closed-form expression due to the assumption that the abundance vectors $\mathbf{a}$ are drawn from a Dirichlet distribution. According to the findings reported by Anandkumar *et al.* [21], our observed reflectance data cross-moments could be explicitly written in terms of α and $\mathbf{S}$ as follows:

$$\begin{aligned} &\mathbf{E}[\mathbf{x}_1 \otimes \mathbf{x}_2] \\ &= \frac{1}{\alpha_0(\alpha_0+1)} \left((\mathbf{S}\alpha \otimes \mathbf{S}\alpha) + \sum_{k=1}^{K} \alpha_k (\mathbf{s}_k \otimes \mathbf{s}_k) \right) \end{aligned} \tag{7}$$

$$\begin{aligned} &\mathbf{E}[\mathbf{x}_1 \otimes \mathbf{x}_2 \otimes \mathbf{x}_3] \\ &= \frac{1}{\alpha_0(\alpha_0+1)(\alpha_0+2)} \end{aligned}$$

$$\times \Bigg((\mathbf{S}\alpha \otimes \mathbf{S}\alpha \otimes \mathbf{S}\alpha) + \sum_{k=1}^{K} \alpha_k (\mathbf{s}_k \otimes \mathbf{s}_k \otimes \mathbf{S}\alpha + \mathbf{s}_k \otimes \mathbf{S}\alpha \otimes \mathbf{s}_k + \mathbf{S}\alpha \otimes \mathbf{s}_k \otimes \mathbf{s}_k) + \sum_{k=1}^{K} 2\alpha_k (\mathbf{s}_k \otimes \mathbf{s}_k \otimes \mathbf{s}_k) \Bigg). \tag{8}$$

After isolating the last two terms in [7] and [8] and applying [20, Th. 3.5], the probabilistic tensor moments can be expressed as a linear combination of $\mathbf{s}_k$

$$M_1 = \sum_{k=1}^{K} \frac{\alpha_k}{\alpha_0} \mathbf{s}_k \tag{9}$$

$$M_2 = \sum_{k=1}^{K} \frac{\alpha_k}{\alpha_0(\alpha_0+1)} (\mathbf{s}_k \otimes \mathbf{s}_k) \tag{10}$$

$$M_3 = \sum_{k=1}^{K} \frac{2\alpha_k}{\alpha_0(\alpha_0+1)(\alpha_0+2)} (\mathbf{s}_k \otimes \mathbf{s}_k \otimes \mathbf{s}_k). \tag{11}$$

C. Tensor Orthogonalization

In order to uncover the spectral signatures $\mathbf{S}$ from the defined probabilistic tensor cross-moments, it is necessary to express these moments as orthogonal matrices, to enable the use of regular tensor decomposition techniques [20]. Let us assume that there is a matrix $\mathbf{W}$ which orthogonalizes the second moment as follows: $M_2(\mathbf{W}, \mathbf{W}) = \mathbf{W}^{\mathrm{T}} M_2 \mathbf{W} = I$, where I represents the identity matrix and T is the transpose operator. In this scenario, the second noncentral moment can be defined by the following expression:

$$\begin{aligned} &M_2(\mathbf{W}, \mathbf{W}) \\ &= \mathbf{W}^{\mathrm{T}} \left(\sum_{k=1}^{K} \frac{\alpha_k}{\alpha_0(\alpha_0+1)} (\mathbf{s}_k \otimes \mathbf{s}_k) \right) \mathbf{W} \\ &= \sum_{k=1}^{K} \mathbf{W}^{\mathrm{T}} \left(\sqrt{\frac{\alpha_k}{\alpha_0(\alpha_0+1)}} \mathbf{s}_k \right) \otimes \left(\sqrt{\frac{\alpha_k}{\alpha_0(\alpha_0+1)}} \mathbf{s}_k \right)^{\mathrm{T}} \mathbf{W} \\ &= \sum_{k=1}^{K} \phi_k \otimes \phi_k^{\mathrm{T}} = I. \end{aligned} \tag{12}$$

As (12) shows, $\phi_k = \mathbf{W}^{\mathrm{T}}((\alpha_k/(\alpha_0(\alpha_0+1))))^{1/2} \mathbf{s}_k$ is a set of orthonormal vectors, since it orthogonalizes M_2. In addition, $\mathbf{s}_k$ can be recovered from ϕ_k, because it is a linear combination of $\mathbf{s}_k$ and $\mathbf{W}$ terms. Similarly, multiplying the third-order probabilistic moment by this ortogonalization matrix, we can obtain the following expression:

$$\begin{aligned} &M_3(\mathbf{W}, \mathbf{W}, \mathbf{W}) \\ &\quad = (\mathbf{W}^{\mathrm{T}} \otimes \mathbf{W}^{\mathrm{T}} \otimes \mathbf{W}^{\mathrm{T}}) M_3 \\ &\quad = (\mathbf{W}^{\mathrm{T}})^{\otimes 3} \left(\sum_{k=1}^{K} \frac{2\alpha_k}{\alpha_0(\alpha_0+1)(\alpha_0+2)} (\mathbf{s}_k \otimes \mathbf{s}_k \otimes \mathbf{s}_k) \right) \\ &\quad = \sum_{k=1}^{K} \frac{2\sqrt{\alpha_0(\alpha_0+1)}}{(\alpha_0+2)\sqrt{\alpha_k}} (\phi_k \otimes \phi_k \otimes \phi_k). \end{aligned} \tag{13}$$

In this letter, we efficiently compute the orthogonalization matrix by using the singular value decomposition (SVD) over the empirical second-order moments as $\hat{M}_2 = A \Sigma A^{\mathrm{T}}$, being $\hat{\mathbf{W}} = A \Sigma^{-\frac{1}{2}}$. After the process, the dimensionality of this third-order tensor can be reduced from $\mathbb{R}^{B \times B \times B}$ to $\mathbb{R}^{K \times K \times K}$.

Algorithm 1 TPM-Based Endmember Extraction

Input x: Quantized HSI data (16-bit)
Input K: Number of endmembers
Output S: Estimated spectral signatures

Compute the empirical moments of $\mathbf{x}$: $\hat{M}_*$
Estimate $\hat{\mathbf{W}}$ using SVD over $\hat{M}_2$: $\hat{\mathbf{W}} \leftarrow A \Sigma^{-\frac{1}{2}}$
Define the third-order tensor: $T \leftarrow M_3(\hat{\mathbf{W}}, \hat{\mathbf{W}}, \hat{\mathbf{W}})$
Conduct the tensor decomposition: TPM(T, L, N)
Recover the spectral signatures: $\mathbf{S} \leftarrow$ Eq. (15)

procedure TPM(T, $L = 100$, $N = 100$)
    for $\tau = 1$ to L **do**
        $\theta_0 \leftarrow$ Random init. from the $\mathbb{R}^K$ unit sphere
        for $t = 1$ to N **do**
            $\theta_t \leftarrow$ Compute the TPM update [Eq. (14)]
        end for
    end for
    Let $\tau^* = \arg\min_{\tau \in [L]} T(\theta_t, \theta_t, \theta_t)$
    Carry out N additional updates over θ_{τ^*} [Eq. (14)]
end procedure

D. TPM for Endmember Estimation

The so-called tensor power method (TPM) decomposition approach [20] is used in this letter to estimate the set of spectral signatures from the corresponding eigenvalues (λ) and eigenvectors (θ). Initially, the aforementioned transformation for tensor orthogonalization and dimensionality reduction is conducted to enable the use of the TPM decomposition over the input HSI data. Being $\mathbf{W}$ the estimated orthogonalization matrix, we define the tensor $T = M_3(\mathbf{W}, \mathbf{W}, \mathbf{W})$ to recover $\mathbf{S}$ by applying a power-deflation approach over T. Specifically, TPM starts with θ_0 randomly sampled from the unit sphere. After several iterations, the power expression update shown in (14) reveals that the largest initialization component dominates the whole iterative process. Note that the $T(\cdot)$ operand generates a tensor by applying the Kronecker product to its arguments

$$\theta_{t+1} = \frac{T(I, \theta_t, \theta_t)}{\|T(I, \theta_t, \theta_t)\|}. \tag{14}$$

Once the θ_k parameter is approximated, λ_k can be recovered from $T(\theta_k, \theta_k, \theta_k) = \lambda_k$. That is, for each pair (θ_k, λ_k), it is possible to recursively compute the tensor $T - (\lambda_k \theta_k \otimes \theta_k \otimes \theta_k)$. Eventually, considering that the $\mathbf{s}_k$ parameter is in the column space of $\mathbf{W}$, the final endmember estimation can be conducted according to (15). Algorithm 1 shows a pseudocode description of the considered TPM-based procedure.

$$\mathbf{s}_k = \frac{\alpha_0 + 2}{2} \hat{\lambda}_k \hat{\mathbf{W}}^{\mathrm{T}} \hat{\theta}_k. \tag{15}$$

III. Experiments

A. Data Sets

Four HSI data sets have been considered in this letter: Synthetic, Samson, Jasper, and Urban. These images have

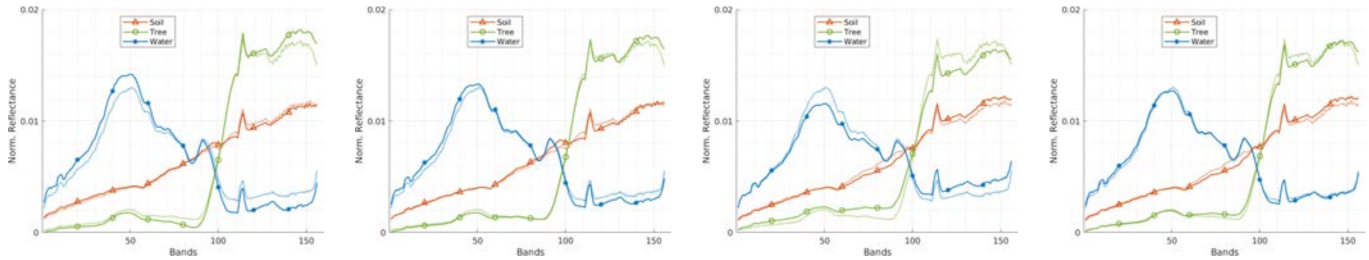

(a) (b) (c) (d)

Fig. 1. Qualitative endmember assessment for the four best methods over the Samson data set. Note that the corresponding ground-truth spectral signatures are plotted using dashed lines and the obtained SAD results are provided in brackets. (a) VCA (0.0634). (b) DEpLSA (0.0427). (c) SCM (0.0723). (d) Proposed (0.0366).

been selected because they are used in multiple reference works in spectral unmixing (see [5], [22]–[25]). Besides, their corresponding ground-truth endmembers are publicly available from https://goo.gl/23ue7v.

1) Synthetic [5] is a simulated HSI scene with 36 × 36 pixels and 224 spectral bands. This simulated data comprises three endmembers which have been selected from the U.S. Geological Survey (USGS) library: Actinolite, Ammonio, and Erionite. This data set has been generated considering an additive Gaussian noise level of 30 dB (SNR), and without including any pure spectral pixels.
2) Samson [23] is a real HSI scene with 95 × 95 pixels and 156 spectral bands, covering from 401- to 889-nm wavelengths. There are three materials in the Samson scene, i.e., soil, tree, and water.
3) Jasper [24] is another real data set which contains 100 × 100 pixels and 198 spectral bands, ranging from 400 to 2500 nm. The Jasper scene contains a total of four endmembers, i.e., road, soil, tree, and water.
4) Urban [25] is a real image with 307 × 307 pixels and 162 bands. These data include four different materials, i.e., asphalt, grass, roof, and tree.

B. Experimental Settings

The performance of our newly proposed approach in the task of uncovering pure spectral signatures from remotely sensed HSI data has been tested against different unmixing methods available in the literature. Specifically, the following endmember extraction algorithms have been considered: VCA [5], MVSA [6], NMF [11], CNMF [12], dual-depth sparse probabilistic latent semantic analysis (DEpLSA) [9], spatial compositional model (SCM) [26] and the proposed approach. All the tested methods have been used considering a given number of endmembers (K) and their corresponding default parameter configurations. Note that K could be also estimated using any subspace identification method [4]. Since this letter is just focused on assessing the spectral signatures, null abundance sparsity constraints have been used in NMF and DEpLSA methods. In the case of the proposed approach, a symmetric Dirichlet concentration parameter $\alpha_0 = 0.2$ has been adopted as a global setting. Regarding the evaluation protocol, the spectral angle distance (SAD) has been employed as a quantitative metric.

C. Results and Discussion

Table I presents the SAD quantitative assessment for the considered unmixing methods (in columns) and data sets (in rows). Note that the last row for each data set contains the corresponding average results and the last row of the table provides the average computational time. Fig. 1 also provides a qualitative evaluation of the four best methods for the Samson collection. In this case, the corresponding ground-truth spectral signatures are visualized using dashed lines.

TABLE I

SAD ENDMEMBER ASSESSMENT (DATA SETS IN ROWS AND UNMIXING METHODS IN COLUMNS)

Dataset	Members	VCA	MVSA	NMF	CNMF	DEpLSA	SCM	Proposed
Synthetic	Actinolite	0.0664	0.0960	0.1621	0.1197	0.0756	0.0836	0.0277
	Ammonio	0.0512	0.1120	0.1439	0.0958	0.0704	0.1538	0.0455
	Erionite	0.0454	0.2264	0.1243	0.0922	0.0418	0.1578	0.0398
	Avg.	0.0543	0.1448	0.1434	0.1026	0.0626	0.1317	**0.0377**
Samson	Soil	0.0288	0.2165	0.2347	0.0401	0.0337	0.0459	0.0440
	Tree	0.0448	0.0805	0.0691	0.0608	0.0300	0.0717	0.0378
	Water	0.1166	0.1927	0.0892	0.2537	0.0646	0.0994	0.0281
	Avg.	0.0634	0.1632	0.1310	0.1182	0.0427	0.0723	**0.0366**
Jasper	Road	0.2008	0.2894	0.4004	0.1852	0.3385	0.7150	0.6333
	Soil	0.1643	0.1702	0.2301	0.1637	0.1446	0.0735	0.0343
	Tree	0.1320	0.2188	0.1957	0.1675	0.0781	0.0700	0.0294
	Water	0.6513	0.4969	0.6761	0.8094	0.0479	0.0822	0.0778
	Avg.	0.2871	0.2938	0.3756	0.3314	**0.1523**	0.2352	0.1937
Urban	Asphalt	0.1269	0.3326	0.3996	0.1012	0.0911	0.2198	0.0943
	Grass	0.2963	0.2292	0.3663	0.1035	0.0491	0.1101	0.0667
	Roof	0.5888	0.6010	0.5889	0.6065	0.3378	0.2082	0.2357
	Tree	0.1792	0.2340	0.2154	0.2721	0.0754	0.0636	0.0496
	Avg.	0.2978	0.3492	0.3926	0.2708	0.1383	0.1504	**0.1116**
Avg. time (s)		3.36	9.35	32.40	59.86	11571.83	38.78	7.86

According to the reported results, it is possible to highlight some important observations. The first noteworthy point is related to the global quantitative performance obtained by the tested methods. As Table I shows, VCA, DEpLSA, and SCM (together with the proposed approach) provide competitive unmixing results for the considered HSI collections. In the case of the Synthetic and Samson scenes, DEpLSA and VCA exhibit a remarkable spectral precision when extracting spectral signatures. However, the proposed approach obtains the best reduction in terms of angular deviation between the estimated endmembers and the corresponding ground-truth ones, being 0.022 and 0.016 radians the improvement over VCA and DEpLSA, respectively. When considering the Jasper data set, DEpLSA, the proposed approach and SCM are the three best methods, obtaining 0.152, 0.194, and 0.235 average SAD values. Finally, the unmixing results in the Urban collection reveal that the proposed approach is the best method, followed by DEpLSA and SCM (for which the SAD is increased 0.027 and 0.039 radians, respectively). Another relevant point arises when analyzing the quantitative endmember results in more detail. As it is possible to observe in Table I, CNMF, VCA, DEpLSA, SCM, and the proposed approach are all able to produce some endmember estimates which are the most similar to the corresponding groundtruth spectral signatures in some cases. However, the proposed approach achieves the most consistent and robust results, since it frequently obtains the best endmember estimation across the all considered HSI images. The qualitative results displayed in Fig. 1 support this observation. More specifically, the proposed approach achieves the most accurate estimation for the water endmember while maintaining a competitive precision for the rest of the spectral signatures. Regarding the computational time, the presented endmember extraction method also exhibits a remarkable performance, being the second most efficient method and significantly better than regular statistical approaches. In general, estimating the endmembers of a given HSI scene raises the challenge of uncovering the most spectrally pure components from mixed data, where the spectral properties of the materials can easily be masked. As a result, HU methods work for mitigating the ill-posed nature of the material dissociation problem by imposing some constraints and assumptions which eventually relieve the uncertainty when uncovering pure spectral signatures. According to the conducted experiments, DEpLSA and SCM rank among the most effective methods. In this sense, the proposed approach considers an analogous statistical perspective, but using a rather different unmixing approach based on tensor moments, which allows us to estimate very competitive endmembers using an unconstrained tensor-based decomposition technique. As a result, the proposed approach allows us to avoid the use of (computationally demanding) optimization algorithms while achieving the benefits provided by a statistical basis.

IV. Conclusion and Future Work

This letter introduces an approach to effectively uncover pure spectral signatures from HSI data using a new probabilistic tensor moment strategy. Whereas conventional statistical models generally provide remarkable unmixing performance using rather complex optimization algorithms, the latest research on tensors points out that this kind of technology is able to obtain competitive results using simpler factorization procedures. In this context, our newly proposed approach integrates a tensor-based decomposition scheme with a probabilistic unmixing framework to take advantage of both technologies when estimating endmembers. The conducted experiments reveal the proposed approach exhibits competitive performance when compared to different state-of-the-art methods available in the literature. Thus, the main conclusion that arises from this work is the potential of the considered third-order probabilistic tensor moments to effectively uncover pure spectral signatures from HSI data. In future, we plan to extend this work to estimate both spectral signatures and fractional abundances from a probabilistic tensor-based perspective. We will also conduct a comparison with traditional tensor-based unmixing methods.

References

[1] P. Ghamisi *et al.*, "Advances in hyperspectral image and signal processing: A comprehensive overview of the state of the art," *IEEE Geosci. Remote Sens. Mag.*, vol. 5, no. 4, pp. 37–78, Dec. 2017.

[2] J. M. Bioucas-Dias, A. Plaza, G. Camps-Valls, P. Scheunders, N. Nasrabadi, and J. Chanussot, "Hyperspectral remote sensing data analysis and future challenges," *IEEE Geosci. Remote Sens. Mag.*, vol. 1, no. 2, pp. 6–36, Jun. 2013.

[3] M. T. Eismann, *Hyperspectral Remote Sensing*. SPIE Bellingham, 2012.

[4] J. M. Bioucas-Dias *et al.*, "Hyperspectral unmixing overview: Geometrical, statistical, and sparse regression-based approaches," *IEEE J. Sel. Topics Appl. Earth Observ. Remote Sens.*, vol. 5, no. 2, pp. 354–379, Apr. 2012.

[5] J. Nascimento and J. Dias, "Vertex component analysis: A fast algorithm to unmix hyperspectral data," *IEEE Trans. Geosci. Remote Sens.*, vol. 43, no. 4, pp. 898–910, Apr. 2005.

[6] J. Li, A. Agathos, D. Zaharie, J. M. Bioucas-Dias, A. Plaza, and X. Li, "Minimum volume simplex analysis: A fast algorithm for linear hyperspectral unmixing," *IEEE Trans. Geosci. Remote Sens.*, vol. 53, no. 9, pp. 5067–5082, Sep. 2015.

[7] J. M. P. Nascimento and J. M. Bioucas-Dias, "Hyperspectral unmixing based on mixtures of Dirichlet components," *IEEE Trans. Geosci. Remote Sens.*, vol. 50, no. 3, pp. 863–878, Mar. 2012.

[8] A. Halimi, N. Dobigeon, J.-Y. Tourneret, and P. Honeine, "A new Bayesian unmixing algorithm for hyperspectral images mitigating endmember variability," in *Proc. IEEE Int. Conf. Acoust., Speech Signal Process. (ICASSP)*, Apr. 2015, pp. 2469–2473.

[9] R. Fernandez-Beltran, A. Plaza, J. Plaza, and F. Pla, "Hyperspectral unmixing based on dual-depth sparse probabilistic latent semantic analysis," *IEEE Trans. Geosci. Remote Sens.*, vol. 56, no. 11, pp. 6344–6360, Nov. 2018.

[10] Y.-X. Wang and Y.-J. Zhang, "Nonnegative matrix factorization: A comprehensive review," *IEEE Trans. Knowl. Data Eng.*, vol. 25, no. 6, pp. 1336–1353, Jun. 2013.

[11] A. Huck and M. Guillaume, "Robust hyperspectral data unmixing with spatial and spectral regularized NMF," in *Proc. 2nd Workshop Hyperspectral Image Signal Process., Evol. Remote Sens.*, Jun. 2010, pp. 1–4.

[12] J. Li, J. M. Bioucas-Dias, A. Plaza, and L. Liu, "Robust collaborative nonnegative matrix factorization for hyperspectral unmixing," *IEEE Trans. Geosci. Remote Sens.*, vol. 54, no. 10, pp. 6076–6090, Oct. 2016.

[13] Y. Qian, F. Xiong, S. Zeng, J. Zhou, and Y. Y. Tang, "Matrix-vector nonnegative tensor factorization for blind unmixing of hyperspectral imagery," *IEEE Trans. Geosci. Remote Sens.*, vol. 55, no. 3, pp. 1776–1792, Mar. 2017.

[14] B. Feng and J. Wang, "Constrained nonnegative tensor factorization for spectral unmixing of hyperspectral images: A case study of urban impervious surface extraction," *IEEE Geosci. Remote Sens. Lett.*, vol. 16, no. 4, pp. 583–587, Apr. 2019.

[15] R. Fernandez-Beltran, F. Pla, and A. Plaza, "Sentinel-2 and sentinel-3 intersensor vegetation estimation via constrained topic modeling," *IEEE Geosci. Remote Sens. Lett.*, vol. 16, no. 10, pp. 1531–1535, Oct. 2019.

[16] R. Fernandez-Beltran, P. Latorre-Carmona, and F. Pla, "Latent topic-based super-resolution for remote sensing," *Remote Sens. Lett.*, vol. 8, no. 6, pp. 498–507, Jun. 2017.

[17] R. Fernandez-Beltran, F. Pla, and A. Plaza, "Intersensor remote sensing image registration using multispectral semantic embeddings," *IEEE Geosci. Remote Sens. Lett.*, vol. 16, no. 10, pp. 1545–1549, Oct. 2019.

[18] R. Fernandez-Beltran and F. Pla, "Sparse multi-modal probabilistic latent semantic analysis for single-image super-resolution," *Signal Process.*, vol. 152, pp. 227–237, Nov. 2018.

[19] R. Fernandez-Beltran, P. Latorre-Carmona, and F. Pla, "Single-frame super-resolution in remote sensing: A practical overview," *Int. J. Remote Sens.*, vol. 38, no. 1, pp. 314–354, Jan. 2017.

[20] A. Anandkumar, R. Ge, D. Hsu, S. M. Kakade, and M. Telgarsky, "Tensor decompositions for learning latent variable models," *J. Mach. Learn. Res.*, vol. 15, no. 1, pp. 2773–2832, 2014.

[21] A. Anandkumar, D. P. Foster, D. J. Hsu, S. M. Kakade, and Y.-K. Liu, "A spectral algorithm for latent Dirichlet allocation," in *Proc. Adv. Neural Inf. Process. Syst.*, 2012, pp. 917–925.

[22] F. Zhu, Y. Wang, B. Fan, S. Xiang, G. Meng, and C. Pan, "Spectral unmixing via data-guided sparsity," *IEEE Trans. Image Process.*, vol. 23, no. 12, pp. 5412–5427, Dec. 2014.

[23] W. He, H. Zhang, and L. Zhang, "Total variation regularized reweighted sparse nonnegative matrix factorization for hyperspectral unmixing," *IEEE Trans. Geosci. Remote Sens.*, vol. 55, no. 7, pp. 3909–3921, Jul. 2017.

[24] R. Liu, L. Zhang, and B. Du, "A novel endmember extraction method for hyperspectral imagery based on quantum-behaved particle swarm optimization," *IEEE J. Sel. Topics Appl. Earth Observ. Remote Sens.*, vol. 10, no. 4, pp. 1610–1631, Apr. 2017.

[25] V. S. K. Ganesan and S. Vasuki, "Maximin distance based band selection for endmember extraction in hyperspectral images using simplex growing algorithm," *Multimedia Tools Appl.*, vol. 77, no. 6, pp. 7221–7237, Mar. 2018.

[26] Y. Zhou, A. Rangarajan, and P. D. Gader, "A spatial compositional model for linear unmixing and endmember uncertainty estimation," *IEEE Trans. Image Process.*, vol. 25, no. 12, pp. 5987–6002, Dec. 2016.